Heliyon 10 (2024) e27303

Contents lists available at ScienceDirect

Heliyon

journal homepage: www.cell.com/heliyon

Research article

Synthesis, characterization, and BSA binding studies of newfangled 2-phenylacetohydrazide derivatives

Muhammad Nawaz Shah [a], Hira Khalid [a,*], Sabina Jhaumeer Laulloo [b], Nausheen Joondan [b], Muhammad Nadeem Arshad [c], Abdullah M. Asiri [c,d], Hassan Butt [a]

[a] Department of Chemistry, Forman Christian College University, Lahore, 54600, Pakistan
[b] Department of Chemistry, University of Mauritius, Reduit, Mauritius
[c] Center of Excellence for Advanced Material Research (CEAMR), King Abdulaziz University, P.O. Box 80203, Jeddah, 21589, Saudi Arabia
[d] Chemistry Department, Faculty of Science, King Abdulaziz University, P.O. Box 80203, Jeddah, 21589, Saudi Arabia

ARTICLE INFO

Keywords:
Phenylacetohydrazide
Single-crystal diffraction
BSA-Binding
Fluorescence spectroscopy

ABSTRACT

Five 2-phenylacetohydrazide derivatives (BPAH = *N*′-benzylidene-2-phenylacetohydrazide, HBPAH = *N*′-(2-hydroxybenzylidene)-2-phenylacetohydrazide), PPAH = 2-phenyl-*N*′-3-phenyl-allylideneacetohydrazide, FMPAH = *N*′-(furan-2-ylmethylene)-2-phenylaceto hydrazide and EPAH = *N*′-ethylidene-2-phenylacetohydrazide were synthesized by the condensation of 2-phenylacetohydrazide with the corresponding aldehyde. The synthesized compounds were characterized by FTIR, 1D, and 2D NMR spectroscopy. The structure of the BPAH and PPAH were analyzed by single crystal X-ray diffraction analysis and in both crystallized compounds, the molecules adopted *trans* geometry around the –C═N- (imine) functional group. To explore the pharmacological significance of these compounds, the binding ability of these compounds with Bovine Serum Albumin (BSA) was investigated using fluorescence spectroscopy. BPAH and PPAH showed the highest binding ability while EPAH, HBPAH, and FMPAH had lower binding ability to BSA molecules. Thermodynamic parameters ΔG, ΔH°, and ΔS° demonstrated that interactions of BSA with compounds BPAH, EPAH, FMAH, and HBPAH were exothermic while for PPAH it was endothermic. The negative enthalpy and entropy of the compounds BPAH, EPAH, FMAH, and HBPAH indicated that van der Waals' forces and hydrogen bonding played a major role in stabilizing the BSA binding with the molecules. Hydrophobic interactions were predominant in the binding of PPAH with BSA tends to interact with two sets of BSA binding sites with an increase in temperature.

1. Introduction

In the post-modern era, numerous efforts are being made by scientists in the development of new compounds with improved efficacy and reduced toxicity, to be considered for pharmaceutical applications. Hydrazones have inspired chemists because of their diverse biological properties such as antimycobacterial [1] anticonvulsant [2], analgesic, anti-inflammatory, antiplatelet aggregation [3], antischistosomal [4], antiviral [5], anti-malarial [6], antimicrobial [7], antihypertensive [8] antitrypanosomal [9] and epidermal

* Corresponding author.
E-mail address: hirakhalid@fccollege.edu.pk (H. Khalid).

https://doi.org/10.1016/j.heliyon.2024.e27303
Received 9 December 2022; Received in revised form 26 February 2024; Accepted 27 February 2024
Available online 18 March 2024

growth factor receptor (EGFR) inhibitory [10].

Hydrazones have more reactive α-hydrogen which is 10 times more acidic than ketones [11]. Their combination with other compounds leads to unique physical and chemical characteristics [12]. Trigonally hybridized nitrogen in the azomethine group has biological importance due to the presence of a lone pair of electrons in sp^2 hybridized orbital [13]. Hydrazones consist of two attached nitrogen atoms of different nature which separates them from other functional groups such as oximes and imines [14] and have a C═N double bond which has conjugation with a terminal nitrogen atom. The physical and chemical properties of hydrazones depend upon these structural fragments. The carbon atom of hydrazones acts as electrophile and as nucleophile while both nitrogen atoms are nucleophilic, whereas the amino nitrogen is more reactive [15]. The most significant reactivity is the nucleophilicity of the carbon-hydrogen atom [16].

The bioactive potential of any compound depends upon its binding interaction with particular binding sites and the molecular structure of enzymes or receptors [17]. The structure of hydrazone has all the required features for biological applications as shown in Fig. 1.

Hydrazone bonds rapidly cleaved in acidic environments such as lysosomes of cells [16]. Therefore, the drug is released in the cell where it performs its function [16]. Hydrolysis can cause cleavage of the imine (N═C) bond and bind drugs in the place of the *R* group which is released at the desired place at certain pH. Hydrazones are stable in the blood where pH is neutral. Hence, cleavage occurs near the tumor area where the pH level is low, and the drug performs different functions such as microtubule misfunctioning and inhibiting protein kinases [18]. This alteration in the *R* group leads to antiviral, anticancer, and anti-inflammatory applications. For the controlled release of drugs, hydrazones are linked to certain drugs for the treatment of cancer such as doxorubicin (DOX) [19]. Serum albumin (SA) is the central protein of the circulatory system which has numerous physiological functions. These proteins maintain the osmotic pressure and pH of blood [20]. In particular, it plays an important role in the deposition and transportation of various endogenous and exogenous compounds and bioactive substances in our bodies [21]. BSA is a globular protein organized in a heart shape comprising three homologous domains (I, II, and III) and six sub-domains (IA and IB). The endogenous and exogenous substances such as metabolites and steroids [22], and fatty acids [20] interact with BSA through these domains. Tyrosine, tryptophan, and phenylalanine contribute to the intrinsic fluorescence of BSA. Principally, two tryptophan residues (Trp 134 and Trp 213) caused the majority of intrinsic fluorescence [22]. Information about drug and plasma proteins interaction is vital to comprehend the pharmacodynamics and pharmacokinetics of a drug [23]. A stable protein-drug complex has a significant impact on the metabolism, distribution, free concentration, toxicity, and efficacy of drugs in the bloodstream [24]. Bovine serum albumin (BSA) is used as a model protein and is studied extensively because 76% of its structure is similar to human serum albumin (HSA) [25,26]. In the current study, a series of 2-phenylacetohydrazide derivatives were synthesized and interactions with BSA were studied using fluorescence spectroscopy.

2. Experimental

2.1. Materials and methods

All chemicals used in this research were of ACS grade and purchased from Sigma Aldrich Chemicals. All the reactions were monitored by TLC plates (Silica gel $60F_{254}$) and spots were visualized through UV light. Chromatograms were developed by using n-hexane and ethyl acetate in different ratios. ^{1}H and ^{13}C NMR spectra of products were recorded at 250 MHz and 62.9 MHz, respectively, on a Bruker Electro Spin NMR spectrometer using DMSO-d_6 as solvent. Chemical shifts were expressed in parts per million (ppm). The FT-IR spectra were obtained with the Agilent Cary 630 FTIR in the range of 600–4000 cm^{-1}. All melting points were taken by Melting Point Tester (GMP-L1) using open capillaries.

2.2. General procedure for the synthesis of 2-phenylacetohydrazide derivatives

Phenylacetohydrazide was stirred with the corresponding aldehyde in the equimolar ratio in different solvents such as toluene, methylene chloride, methanol, and diethyl ether (Fig. 2). The reaction was monitored by TLC (*n*-hexane/ethyl acetate, 1:1). The details

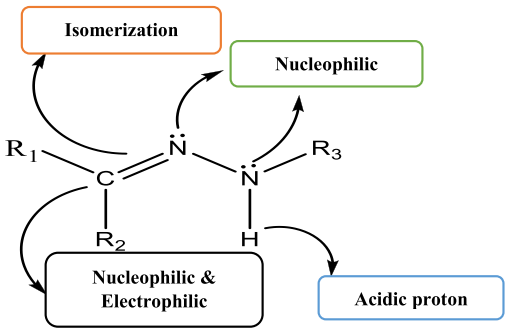

Fig. 1. Functional diversity of hydrazone moiety (Ali et al., 2020).

of the solvent effect on reaction time are tabulated in Table 1. The crude product was washed with cold n-hexane (10 mL) and recrystallized from ethanol (see Fig. 3).

2.2.1. N′-benzylidene-2-phenylacetohydrazide (BPAH)

Yield (0.21 g, 93%), Light yellow crystals; M.P: 147–149 °C; IR υ_{max} (cm^{-1}): 3220 (N–H), 3065 (=C–H), 2963 (-C-H), 1656 (C═N), 1650 (C═O). ^{1}H NMR (250 MHz, DMSO-d_6), δ (ppm): 11.60 (s, 1H, OH-enol), & 11.34 (s, 1H, NH), 8.17 & 7.96 (s, 1H, H-7), 7.62–7.67 (m, 2H, H-9 & H-13), 7.38–7.41 (m, 3H, H-10 to H-12), 7.22–7.29 (m, 4H, H2 to H-5), 7.18–7.21 (m, 1H, H-6), 3.44 (s, 2H, CH_2-enol) & 3.95 (s, 2H, CH_2-keto). ^{13}C NMR (250 MHz, DMSO-d_6), δ (ppm): 167.1, 172.8 (C═O), 143.4 & 147.1 (C7), 136.2 (C1), 134.7 (C8), 130.2 (C11), 129.8 (C6), 129.5 (C2), 129.3 (C10 & C12), 128.8 (C5), 128.7 (C3), 127.5 (C9), 127.2 (C13), 126.8 (C4), 39.4 & 41.6 (CH_2).

2.2.2. N′-(2-hydroxybenzylidene)-2-phenylacetohydrazide (HBPAH)

Yield (0.746 g, 88%), M.P: 178–180 °C; light brown crystals; IR υ_{max} (cm^{-1}): 3285.6 (N–H stretch), 3211.1 (=C–H stretch), 3035.9 (-C-H stretch), 1656.8 (C═N stretch), 1644 (C═O stretch). ^{1}H NMR (250 MHz, DMSO-d_6), δ (ppm): 11.86 (s, 1H, OH-enol), & 11.29 (s, 1H, NH), 9.19 (bs, 1H, H-9), 8.37 & 8.25 (s, 1H, H-7), 7.45–7.67 (dd, 5,1.4Hz, 1H, H-12), 6.88–6.83 (d, 1H, H-13) 7.16–7.30 (m, 5H, H2 to H-6, H10 to H-11), 7.18–7.21 (m, 1H, H-6), 3.52 (s, 2H, CH_2-enol) & 3 0.91 (s, 2H, CH_2-keto). ^{13}C NMR (250 MHz, DMSO-d_6), δ (ppm): 172.4, 170.0 (C═O), 157.6, 156.8 (C7), 136.7 (C1), 119.1 (C8), 131.8 (C11), 129.6 (C6), 129.8 (C2), 116.8 (C10), 119.8 (C12), 128.8 (C5), 129.4 (C3), 166.9 (C9), 131.5 (C13), 128.6 (C4), 38.8, 42.2 (CH_2).

2.2.3. 2-Phenyl-N′-(3-phenylallylidene)acetohydrazide (PPAH)

Yield (0.21 g, 93%), M.P: 182–184 °C; Pale yellow crystals; IR υ_{max} (cm^{-1}): 3173.8 (N–H), 3062 (=C–H), 2953.9 (-C-H), 1662.4 (C═N), 1650 (C═O). ^{1}H NMR (250 MHz, DMSO-d_6), δ (ppm): 11.60 (s, 1H, OH-enol), 11.34 (s, 1H, NH), 7.67 (d, 1H, H-7), 7.48–7.52 (d, 8Hz, 2H, H-10 & H-14), 7.22–7.26 (m, 5H, H-2 to H-6 & H-12), 7.25 (tt, 7.4, 1.3Hz, 1H, H-13), 7.02 (d, 15Hz, 1H, H-9), 6.89–6.91 (m, 1H, H-15), 6.45 (dd, 15, 10Hz, 1H, H-8), 3.44 (s, 2H, CH_2-enol) & 3.79 (s, 2H, CH_2-keto). ^{13}C NMR (62.9 MHz, DMSO-d_6), δ (ppm): 172.4, 170.0 (C═O), 157.6, 156.8 (C7), 136.0 (C1), 119.1 (C8), 131.8 (C11), 129.6 (C6), 129.8 (C2), 116.8 (C10), 119.8 (C12), 128.8 (C5), 129.4 (C3), 166.9 (C9), 131.5 (C13), 128.6 (C4), 38.8, 42.2 (CH_2).

2.2.4. N′-(furan-2-ylmethylene)-2-phenylacetohydrazide (FMPAH)

Yield (0.50 g. 66%), M.P: 160–162 °C; bright yellow crystals; IR υ_{max} (cm^{-1}): 3201.8 (N–H), 3151.6 (=C–H), 3060.1 (-C-H), 1664.3 (C═N), 1640 (C═O)·^{1}H NMR (250 MHz, DMSO-d_6), δ (ppm): 11.53 (s, 1H, OH-enol), 11.29 (s, 1H, NH), 8.06, 7.85 (s, 1H, H-7), 7.48–7.52 (d, 8Hz, 2H, H-10 & H-14), 7.17–7.29 (m, 5H, H-2 to H-6), 6.83–6.85 (d, 3.4Hz, 1H, H-10), 6.56–6.59 (dd, 3.4, 1.9Hz, 1H, H-11), 7.77 (d, 4Hz, 1H, H-12), 3.87 (s, 2H, CH_2-keto) & 3.48 (s, 2H, CH_2-enol). ^{13}C NMR (62.9 MHz, DMSO-d_6), δ (ppm): 172.6, 167.0. (C═O), 149.8 (C9), 149.6 (C7), 145.3 (C12), 136.0 (C1), 130 (C2), 129.5 (C6), 128.8 (C3), 128.7 (C5), 127.1 (C4), 112.5 (C10), 113.5 (C11), 39.4, 41.6 (CH_2).

2.2.5. N′-ethylidene-2-phenylacetohydrazide (EPAH)

Yield (0.31 g, 53%), M.P: 124–127 °C; light brown crystals; IR υ_{max} (cm^{-1}): 3295 (N–H), 3203 (=C–H), 3032.2 (-C-H) 1640 (C═N), 1650 (C═O). ^{1}H NMR (250 MHz, DMSO-d_6), δ (ppm): 11.30 (s, 1H, NH), 7.27–7.34 (m, 5H, H-2 & H-6), 7.06 (q, 6.9Hz, 1H, H-7), 3.77 (s, 2H, CH_2 keto), 1.86 (d, 6.9Hz, 3H, CH_3). ^{13}C NMR (62.9 MHz, DMSO-d_6), δ (ppm): 167.1 (C═O), 148.4 (C7), 136.1 (C1), 129.8 (C2 & C6), 128.4 (C3 & C5), 127.8 (C4), 38.8, 42.2 (CH_2), 18.5 (C8).

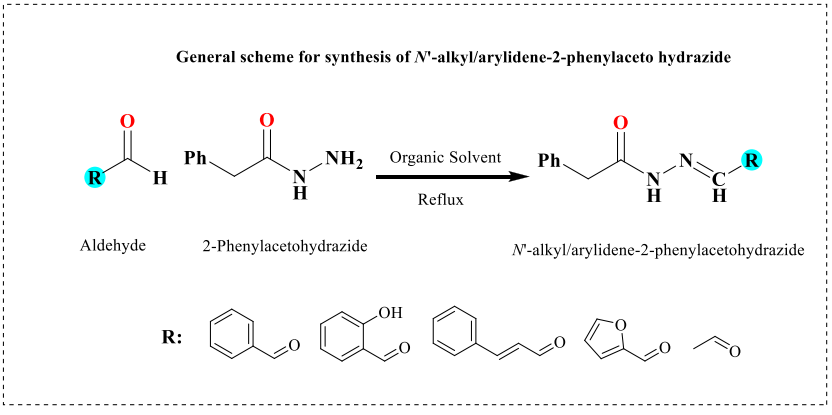

Fig. 2. General scheme for the synthesis of 2-phenylacetohydrazide derivatives.

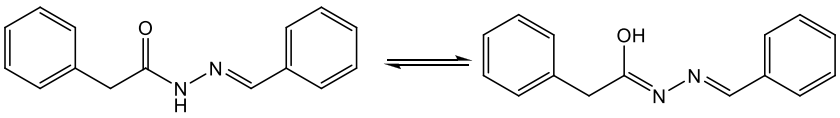

Keto **Enol**

Fig. 3. Tautomeric forms of phenylacetohydrazide.

Table 1
Synthesis of hydrazones from 2-phenylactohydrazide and aldehydes in various solvents.

Code	Aldehyde	Solvent	Reaction Time (hours)	Yield (%)
BPAH	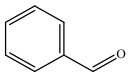	Tol	2.5	93
HBPAH	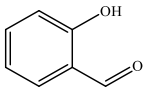	Tol	26	88
PPAH	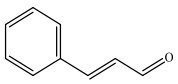	Tol	12	93
FMPAH	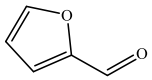	Tol	6	96
EPAH	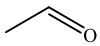	Tol	5.8	53
HBPAH	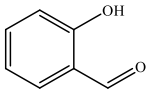	DCM	18	85
EPAH	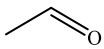	DCM	12	86
BPAH	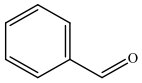	MeOH	1.3	74
HBPAH	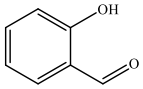	MeOH	2	84
PPAH	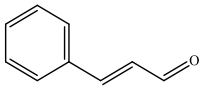	MeOH	8.5	96
FMPAH	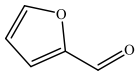	MeOH	3.5	95
EPAH	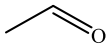	MeOH	13.2	82
BPAH	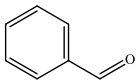	Et2O	9.5	90
FMPAH	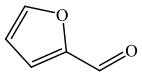	Et2O	10	88

2.3. X-ray diffraction study

The two compounds PPAH and BPAH from the series of intentional designed materials were crystalized with good enough shapes to obtain their single crystals analysis by their diffraction under X-rays, Proper sized single crystals were mounted on Agilent SuperNova (Dual source) Agilent Technologies Diffractometer, equipped with microfocus Cu/Mo Kα radiation for data collection. The data collection was accomplished using CrysAlisPro software [27]. at 296 K under the Mo Kα radiation. The structure solution was performed using SHELXS–97 method [28]. and refined by full–matrix least–squares methods on F^2 using SHELXL–97 method, in-built with WinGX [29]. All non–hydrogen atoms were refined anisotropically by full–matrix least squares methods [28]. The figures were generated through *PLATON* [30]. and *ORTEP* [36]. in built with WinGX [29].

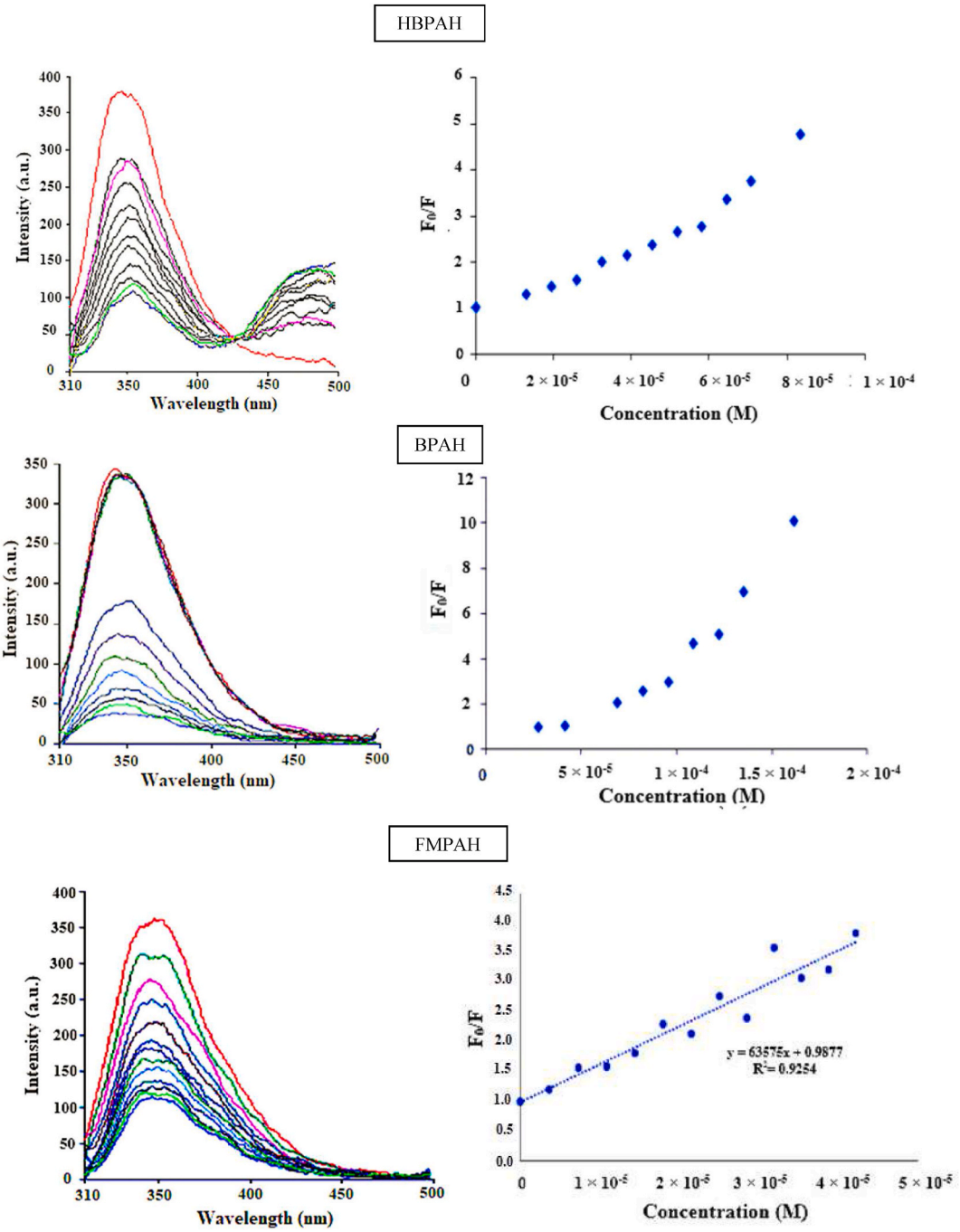

Fig. 4. Fluorescence intensity results with increasing concentration of phenylacetohydrazide derivatives HBPAH, BPAH and FMPAH.

For both compounds, aromatic C–H hydrogen atoms have been positioned geometrically and treated as riding atoms with C–H = 0.93 Å and U_{iso}(H) = 1.2 U_{eq}($C_{aromatic}$). For methylene groups C–H hydrogen atoms were also positioned geometrically where C–H = 0.97 Å and U_{iso}(H) = 1.2 U_{eq}($C_{methylene}$). For PPAH the N–H hydrogen atoms were positioned geometrically with N–H = 0.86(2) Å while for BPAH the N–H were positioned with fourier map N–H = 0.89(2) Å. The U_{iso}(H) value in each case was set to 1.2 U_{eq}(C_{N-H}). The Crystal data was deposited at the Cambridge Crystallographic Data Centre and following deposition number (CCDC numbers) has been allocated as CCDC number 1989985–1989,986 for PPAH and BPAH, respectively. Crystal data can be received free of charges on application to CCDC 12 Union Road, Cambridge CB21 EZ, UK. (Fax: (+44) 1223 336–033; e-mail: data_request@ccdc.cam. ac. uk).

2.4. In BSA binding studies fluorescence measurements

For the determination of the BSA quenching constant, fluorometric titration of BSA solution (1 mL, 10 μM) in phosphate buffer (2 mL) with stock solution of 2-phenylacetohydrazide derivatives were carried out using fluorescence measurements. The solutions were excited at 295 nm and the intensity of the BSA solutions with and without the phenyl acetohydrazide were recorded at 336 nm. In order to eliminate the influence of the inner filter effect (IFE) on the Stern-Volmer plots, the steady-state fluorescence spectra were corrected with the help of the following formula [1] [26]:

$$F_{cor} = F_{obs} \bullet 10^{(Aex+Aem)/2} \quad (1)$$

where, F_{obs} is the measured fluorescence intensity. F_{cor} is the corrected fluorescence intensity. A_{ex} and A_{em} are the absorbance of the mixed solution at λ_{ex} and λ_{em}, respectively.

For the thermodynamics studies, the experiment was repeated and was performed at different temperatures 298, 308, and 313 K.

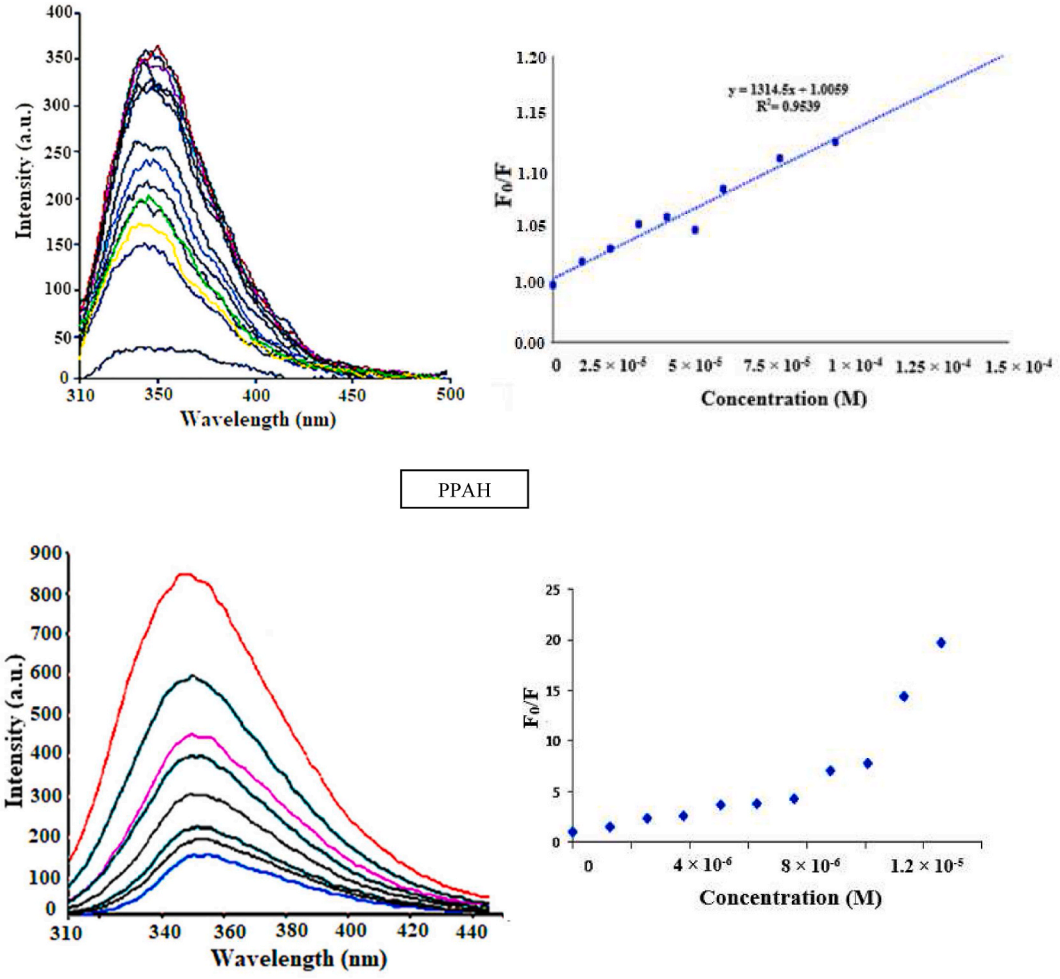

Fig. 5. Fluorescence intensity results with increasing concentration of phenylacetohydrazide derivatives EPAH and PPAH.

3. Results and discussion

3.1. Chemistry

Synthesis of phenylacetohyrazide derivatives was achieved by the treatment of 2-phenylacetohyrazide with appropriate aldehydes in different solvents using a simple one-pot reaction. (Table 1).

The structures of the hydrazides were established based on the appearance of an NH absorption band in the 3295–3151 cm^{-1} region and a carbonyl function band in the 1664-1645 cm^{-1} region of their IR spectra.

The NMR data were concordant with the structures proposed for the different compounds and the data are given in the experimental section. The detailed assignment of the different protons and carbons for compounds BPAH and FMPAH is based on 1D and 2D NMR data (Figs. S2–S5 Tables S1–S2). The ^1H NMR spectra displayed two broad singlets in the region 11.60, 11.34 and 11.86, 11.53 due to the presence of keto-OH and NH indicating that these hydrazides exist in the *keto-enol* tautomers in solution Fig. 3 [38]. The fact that the hydrazides exist in two forms is also confirmed by the appearance of two azomethines (CH═N), two CH_2, and two carbonyl signals (Table S1 &S2).

3.2. BSA binding studies

The fluorescence emission spectra of BSA in the presence and absence of the phenylacetohydrazide derivatives were recorded at an emission of $\lambda = 334$ nm (excited at $\lambda = 295$ nm) to study the changes occurring in the microenvironment of the serum albumin. A decrease in the fluorescence intensity was observed with increasing concentration of phenylacetohydrazide derivatives due to the formation of the non-fluorescent complex between the BSA molecule and the phenylacetohydrazide derivatives (Figs. 4 and 5). Fluorescent quenching can occur via three mechanisms, namely static, dynamic and a combined dynamic and static mechanisms. Static quenching mechanism involves the formation of ground-state complex of the protein with the quencher, while dynamic quenching is caused by the collision of the protein with the quencher. In the case of combined dynamic and static quenching, the protein undergoes both collision and complex formation with the quencher [31]. Static and dynamic quenching mechanism can be identified by studying the dependence of the binding with temperature. In static quenching mechanism, the quenching constant (K_{sv}) decreases with an increase in temperature while in the case of dynamic quenching, the value of K_{sv} increases with increasing temperature. The quenching mode was analyzed using the Stern-Volmer equation (Equation (2)).

$$F_o / F = 1 + Kq\tau 0\,[Q] = 1 + K_{sv}\,[Q] \quad (2)$$

where F_0 and F represent the steady-state fluorescence intensities in the absence and the presence of the 2-phenylacetohydrazide derivatives, respectively. K_q is the bimolecular quenching constant of the reaction and K_{sv} is the Stern-Volmer quenching constant which indicates the kinetics involved in the quenching of BSA in the presence of the 2-phenylacetohydrazide derivatives. The values of K_{sv} and K_q in Table 2 give an overview of the mechanism of binding, *i.e.* either static or dynamic process. [Q] and τ0 correspond to the concentration of the compounds and the average lifetime of the pure BSA molecules (10^{-8} s), respectively.

From Fig. 4, it can be seen that the dependence of F_o/F on [Q] is linear in the case of FMPAH and EPAH which indicates that the quenching can be dynamic or static. However, in the case HBPAH, BPAH, and PPAH, the dependence of F_o/F on [Q] is nonlinear, indicating the possibility of a combined dynamic and static quenching mechanism. At a lower concentration of the quencher, the F_o/F showed an almost linear dependence with the concentration of HBPAH, BPAH and PPAH and therefore treated according to the Stern-Volmer Equation (1), in a similar way to that of Wang et al. [32]. The calculated K_q values (Table 2) are larger than the maximum scattering collision quenching rate constant ($2 \times 10^{10}\ M^{-1}\ s^{-1}$) in dynamic quenching, which indicates that the quenching of BSA with the phenylacetohydrazide derivatives follows a static process [33], rather than a dynamic one. The quenching mechanism was further confirmed by determining the K_{SV} of the interaction of the phenylacetohydrazide derivatives with BSA at different temperatures.

Table 2
The Stern-Volmer quenching constant (K_{SV}) and bimolecular quenching constant (k_q) at different temperatures.

Compounds	Temperature (K)	n	K_{SV} (M)	K_q ($\times 10^{12}$)
HBPAH	298	1.30	4.12×10^4	4.12
	308	1.10	7.73×10^3	0.77
	313	0.68	6.12×10^4	6.12
BPAH	298	2.15	6.13×10^4	6.13
	308	1.49	4.41×10^4	4.41
	313	1.14	4.68×10^4	4.68
FMPAH	298	0.98	6.35×10^4	6.35
	308	0.69	1.69×10^4	1.69
	313	0.35	1.08×10^4	1.08
EPAH	298	1.94	2.13×10^3	0.21
	308	0.85	1.31×10^3	0.13
	313	0.79	1.22×10^3	0.12
PPAH	298	1.4	4.46×10^5	44.6
	308	1.7	6.64×10^5	66.4
	313	1.7	7.49×10^5	74.9

FMPAH and EPAH showed a decrease in K_{SV} values with increasing temperature, which confirms a static quenching mechanism [34]. It was initially found that HBPAH, BPAH and PPAAH have a likelihood of combined static and dynamic quenching as shown by their non-linear Stern-Volmer plot. An increase temperature from 298 K to 308 K showed a decrease K_{SV} values for both HBPAH, BPAH, which then increase with a further increase in temperature till 313 K, which indicates the possibility of a combined static and dynamic quenching mechanism. However, the K_{SV} of PPAH was found to increase with a rise in temperature which suggests the quenching process is initiated by a dynamic mechanism.

The affinity between a drug and a receptor is determined by its binding constant, K_b. Since the quenching of the fluorescence of BSA

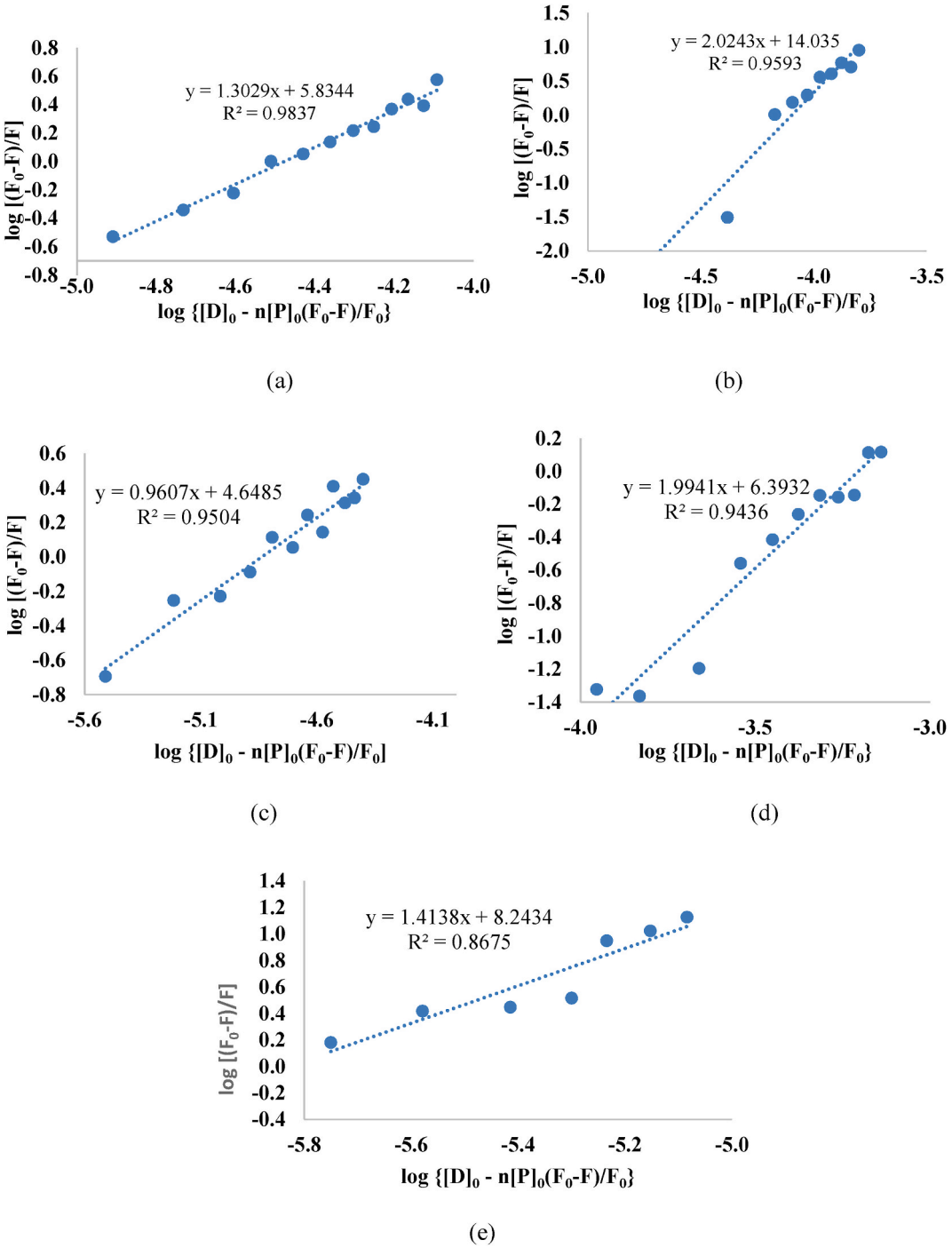

Fig. 6. Double logarithmic plots of the binding of (a) HBPAH, (b) BPAH, (c) FMPAH, (d) EPAH and (e) PPAH.

by the phenylacetohydrazide derivatives was mostly via static mechanism, the binding process might involve the formation of a non-fluorescent complex between BSA and the phenylacetohydrazide derivative. Hence, the fluorescence data were treated using the equation reported by Kou et al. [34] (Equation (3)). to obtain the binding constant K_b and number of binding site, n.

$$\text{Log}\ (F_0 - F)\ / F = \log K_b + n \log \left\{[D]_0 - n[P]_0(F_0 - F) / F_0\right\} \quad (3)$$

where $[P]_0$ is the total concentration of the protein, that is BSA; $[D]_0$ is the total concentration of drug (phenylacetohydrazide derivative); F_0 and F refer to the fluorescence intensities of free BSA solution and the mixture solution of BSA and the phenylacetohydrazide derivatives and n is the number of binding sites of the BSA to the phenylacetohydrazide derivatives.

The K_b values obtained indicate the plasma distribution of the compounds being studied. Weak binding can lead to a short lifetime or poor distribution of the compounds while the strong binding is responsible for the reduction in the plasmatic concentration of the compounds. In general, the compounds displayed moderate to good binding ability with BSA. Comparing the K_b values at 298 K, BPAH and PPAH showed the highest binding ability with BSA due to the presence of two aromatic moieties which might provide additional interaction with BSA via hydrophobic interaction or π-π interaction. However, the presence of a phenolic group in HBPAH was found to cause a decrease in the binding constant, indicating that the OH group did not favor the interaction between the compound and BSA. The presence of a furan moiety was found to lower the binding constant of FMPAH compared to EPAH. BPAH and EPAH were found to bind to two binding sites of BSA molecule at 298 K (Fig. 6a–e).

3.2.1. *Thermodynamics of binding*

The driving forces for the binding of small molecules to BSA mainly involve hydrogen bonding, van der Waals, electrostatic, and hydrophobic interactions. These interactions can be described by thermodynamic parameters such as free energy (ΔG), enthalpy (ΔH), and entropy (ΔS) and used to determine the type of binding taking place between the compounds under investigation and BSA. There are 3 sets of conditions for ΔH and ΔS that can be used to indicate the type of interaction in BSA binding [41]. When $\Delta H > 0$ and $\Delta S > 0$, hydrophobic interactions play a major role in the binding. If $\Delta H < 0$ and $\Delta S > 0$ electrostatic interactions are more prominent and when $\Delta H < 0$ and $\Delta S < 0$, van der Waals and hydrogen bonding are more important.

To characterize the binding forces of the 2-phenylacetohydrazide derivatives to BSA, the thermodynamic parameters of binding were determined at 298, 308, and 313 K. The values for ΔH, ΔS, and ΔG were calculated using equations (4) and (5).

$$\Delta G = - \text{RT} \ln K_b \quad (4)$$

where T is the absolute temperature, K_b is the binding constant at temperature T, and R is the gas constant. The values of ΔH and ΔS can be analyzed based on the van't Hoff's formula:

$$\ln k_b = -\frac{\Delta H}{\text{RT}} + \frac{\Delta S}{\text{R}} \quad (5)$$

where T is the absolute temperature, K_b is the binding constant, and R is the gas constant.

The value of ΔG was then calculated using Equation (6).

$$\Delta G = \Delta H - \text{T}\Delta S \quad (6)$$

From Table 3, it can be observed that all five compounds displayed negative ΔG values, implying that their complex formation with BSA occurs spontaneously at all temperatures.

From the ΔH° and ΔS° values, it can be deduced that the binding of HBPAH, BPAH, FMPAH, and EPAH occurs mainly via van der Waals forces and hydrogen bonding, while the binding of PPAH to BSA occurs mainly via electrostatic interactions. In the case of BPAH and EPAH, an increase in temperature favors the binding of the compounds to only one binding site (Fig. 7a–e).

Table 3
Thermodynamic parameters of the interaction between BSA and the 2-phenylacetohydrazide derivatives in phosphate buffer.

Compounds	Temperature (K)	n	K_b (M^{-1})	ln K_b	ΔG (kJmol^{-1})	ΔH° (kJmol^{-1})	ΔS° (Jk-^{1} mol^{-1})
HBPAH	298	1.30	6.83×10^5	13.43	−33.27		
	308	1.09	1.41×10^4	9.56	−24.46	−385.1	−1178
	313	0.59	2.89×10^2	5.67	−14.74		
BPAH	298	2.00	1.08×10^{14}	32.32	−80.03		
	308	1.48	6.75×10^6	15.73	−40.25	−937.3	−2885
	313	1.44	4.56×10^6	15.33	−39.88		
FMPAH	298	0.96	4.45×10^4	10.70	−26.51		
	308	0.74	1.13×10^3	7.03	−17.99	−318.4	−978
	313	0.52	8.22×10^1	4.41	−11.47		
EPAH	298	1.99	2.47×10^6	14.72	−35.45		
	308	0.88	4.12×10^2	6.02	−15.41	−504.9	−1575
	313	0.83	2.47×10^2	5.51	−14.33		
PPAH	298	1.41	1.75×10^8	18.98	−47.00		
	308	1.50	1.11×10^8	18.52	−47.41	−3619.9	56
	313	1.47	9.96×10^7	18.42	−47.90		

3.3. Crystal structure characterization

The two compounds were crystalized for characterization and to support our synthesis procedures. The aim was to know the expected interactions among the atoms or molecules in the crystals of the compounds. In the compound PPAH allylidene-hydrazide backbone (N1/N2/C9/C10/C11) relates to the phenyl acetyl (C1/C2/C3/C4/C5/C6/C7/C8/O1) group on the nitrogen atom (N1) while phenyl ring is attached on another side of this backbone on carbon (C11) atom Fig. 8 and Table 4. The two aromatic rings (C1–C6) and (C12–C17) are oriented at a dihedral angle of 62.53(5)°. The plane produced from the joined atoms of the backbone (N1/

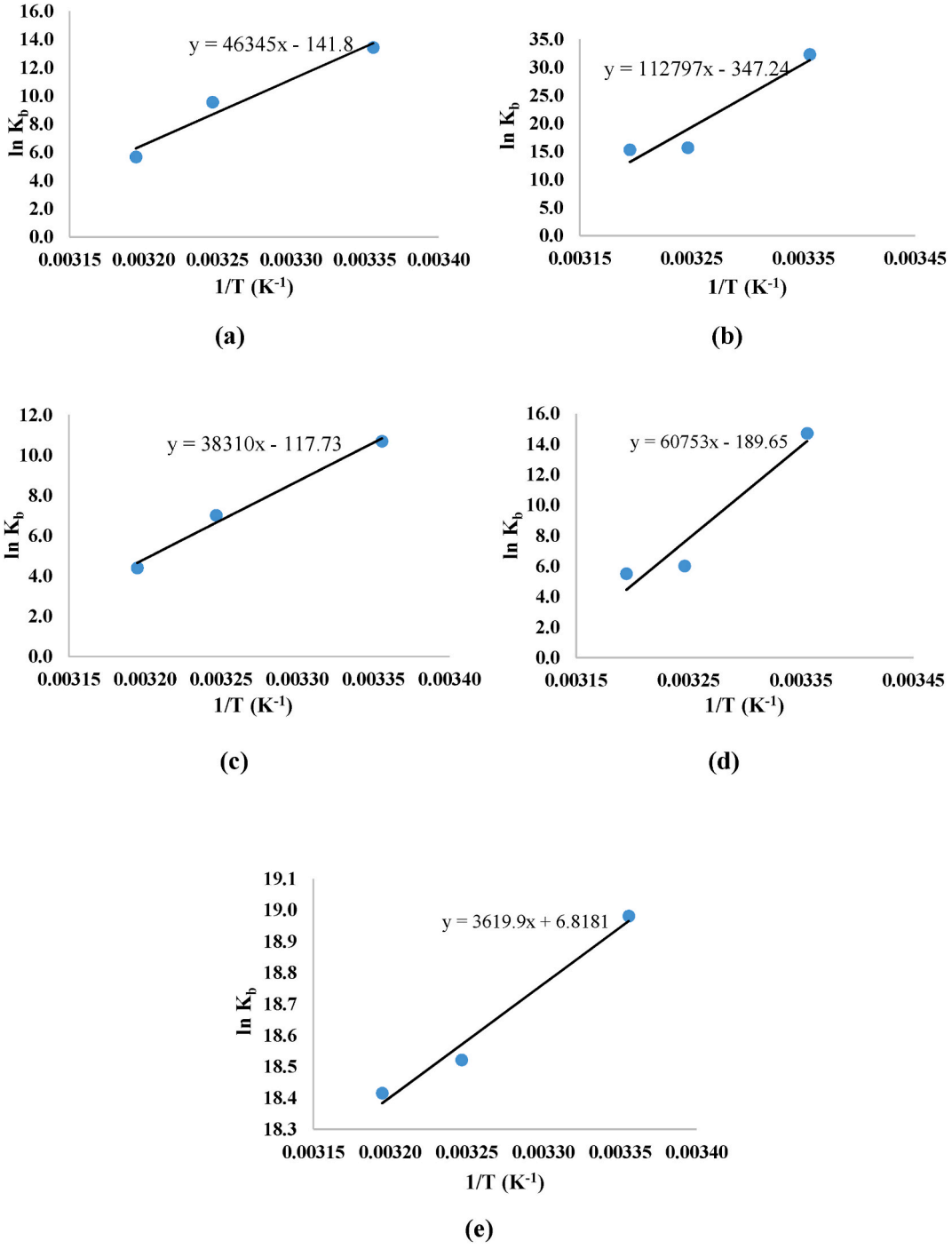

Fig. 7. Van't Hoff Plots for the BSA-2-phenylacetohydrazide derivatives system (a) HBPAH, (b) BPAH, (c) FMPAH, (d) EPAH, (e) PPAH.

N2/C9/C10/C11) is almost planar with the root mean square deviation of 0.0311(7) Å where the most deviations were observed from C11 [0.0341 (7 Å)] and C9 [−0.0483 (12)Å]. The aromatic rings (C1–C6) and (C12–C17) deviated by 67.78(72)° and 9.87(13)° with the plane produced from the atoms of backbone-chain (N1/N2/C9/C10/C11). In this structure hydrogen bonding interaction (Table 5), N1–H1N ….O1, generates the dimers and forms an eight-membered ring motif R_2^2 (8) Fig. 9 and Fig. S10 following the symmetry operation -x+3, -y+1, -z+1, Table 4. Bond lengths, bond angles, and torsion angles for both compounds are comparable with each other and represented in Tables S3 and S4 respectively. In the compound, BPAH methyl-hydrazide backbone (N1/N2/C9) is connected with the phenyl acetyl (C1/C2/C3/C4/C5/C6/C7/C8/O1) group on the nitrogen atom (N1) while phenyl ring is attached on another side of this backbone on carbon (C9) atom Fig. 10. The two aromatic rings (C1–C6) and (C10–C15) are oriented at a dihedral angle of 72.93(82)°. The plane produced from the joined atoms of the backbone (N1/N2/C9) is almost planar with the root mean square deviation of 0.000(7) Å. The aromatic rings (C1–C6) and (C10–C15) deviated by 74.23(12)° and 2.82(25)° with the plane produced from the atoms of backbone-chain (N1/N2/C9). Like the PPAH, in this structure N1–H1N ….O1 hydrogen bonding interaction to involve generate the dimers and form eight-membered ring motif R_2^2 (8) Fig. 11 and Fig. S15, following the symmetry operation -x+2, -y+2, -z, Table S12 and this is like other compounds having related functionality [35,36]. The hydrogen bonding interactions have been counterchecked by Hirshfeld surface analysis and it is confirmed that there is dimerization among the molecules in both the compounds Figs. S3 and S4 [37].

4. Conclusion

The current study was performed to synthesis five 2-phenylacetohydrazide derivatives. The synthesized compounds were structurally elaborated through ^{1}H NMR, ^{13}C NMR IR, and X-ray diffraction techniques. The crystal structures have been analyzed for two compounds. The dihedral angles between the different planes of the molecules have been discussed. The N–H···O type hydrogen bonding interactions involved in the formation of dimers to stabilize the crystallinity of the compounds. The new crystal structures submitted to the Cambridge Crystallographic Data Centre (CCDD). The BSA binding study revealed the excellent binding potential of synthesized compounds.

Data availability statement

The Crystal data was deposited at the Cambridge Crystallographic Data Centre and following deposition number (CCDC numbers) has been allocated as CCDC number 1989985–1989,986 for PPAH and BPAH, respectively. Crystal data can be received free of charges on application to CCDC 12 Union Road, Cambridge CB21 EZ, UK. (Fax: (+44) 1223 336–033; e-mail: data_request@ccdc.cam. ac. uk).

CRediT authorship contribution statement

Muhammad Nawaz Shah: Project managment, conducting experiemntation, characterization, Investigation, analysis, Conceptualization, Writing – review & editing, Software. **Hira Khalid:** Writing – review & editing, Writing – original draft, Visualization, Validation, Supervision, Software, Resources, Project administration, Methodology, Investigation, Conceptualization. **Sabina Jhaumeer Laulloo:** Writing – review & editing, Writing – original draft, Validation, Software, Resources, Methodology, Formal analysis, Data curation. **Nausheen Joondan:** Writing – review & editing, Writing – original draft, Visualization, Validation, Software, Resources, Investigation, Formal analysis, Data curation. **Muhammad Nadeem Arshad:** Writing – review & editing, Writing – original draft, Visualization, Validation, Software, Methodology, Investigation, Formal analysis, Data curation. **Abdullah M. Asiri:** Software, Resources, Project administration, Funding acquisition, Muhammad Nawaz Shah, Writing – original draft, Visualization, Methodology, Investigation, Formal analysis. **Hassan Butt:** Methodology, Investigation.

Declaration of competing interest

The authors declare that they have no known competing financial interests or personal relationships that could have appeared to influence the work reported in this paper.

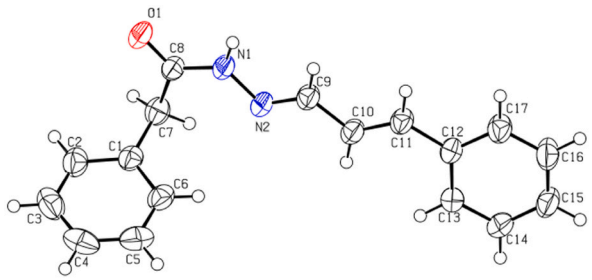

Fig. 8. *ORTEP* diagram of (PPAH), where thermal ellipsoids were drawn at 40% probability level.

Table 4
Crystal data and structure refinement for PPAH and BPAH.

Identification code	(PPAH)	(BPAH)
CCDC Number	1989985	1989986
Empirical formula	$C_{17}H_{16}N_2O$	$C_{15}H_{14}N_2O$
Formula weight	264.32	238.28
Temperature/K	296(2)	296(2)
Crystal system	monoclinic	monoclinic
Space group	$P2_1/c$	$P2_1/n$
a/Å	6.4604(3)	5.034(2)
b/Å	25.5538(13)	10.165(4)
c/Å	8.4831(5)	24.83(3)
α/°	90	90
β/°	90.541(4)	91.098(4)
γ/°	90	90
Volume/Å^3	1400.39(13)	1270.7(16)
Z	4	4
ρ_{calc}g/cm^3	1.254	1.246
μ/mm^{-1}	0.079	0.080
F(000)	560.0	504.0
Crystal size/mm^3	0.28 × 0.14 × 0.09	0.48 × 0.12 × 0.09
Radiation	MoKα (λ = 0.71073)	MoKα (λ = 0.71073)
2θ range for data collection/°	5.764 to 58.384	6.348 to 58.874
Index ranges	$-8 \le h \le 8$, $-30 \le k \le 33$, $-11 \le l \le 10$	$-6 \le h \le 6$, $-13 \le k \le 13$, $-33 \le l \le 22$
Reflections collected	11,500	9467
Independent reflections	3427 [$R_{int} = 0.0241$, $R_{sigma} = 0.0274$]	3093 [$R_{int} = 0.0418$, $R_{sigma} = 0.0455$]
Data/restraints/parameters	3427/0/181	3093/0/166
Goodness-of-fit on F^2	1.042	1.110
Final R indexes [I ≥ 2σ (I)]	$R_1 = 0.0468$, $wR_2 = 0.1053$	$R_1 = 0.0503$, $wR_2 = 0.1190$
Final R indexes [all data]	$R_1 = 0.0702$, $wR_2 = 0.1210$	$R_1 = 0.0960$, $wR_2 = 0.1463$
Largest diff. peak/hole/e Å^{-3}	0.13/-0.19	0.16/-0.21

Table 5
Hydrogen bonds for PPAH and BPAH.

PPAH						
D	H	A	d(D-H)/Å	d(H-A)/Å	d(D-A)/Å	D-H-A/°
N1 [1]3-X,1-Y,1-Z	H1N	O1[a]	0.86	2.11	2.9636(17)	175.0
BPAH						
D	**H**	**A**	**d(D-H)/Å**	**d(H-A)/Å**	**d(D-A)/Å**	**D-H-A/°**
N1	H1	O1[a]	0.86(2)	2.03(2)	2.895(3)	175.3(18)

[a] 2-X,2-Y,-Z.

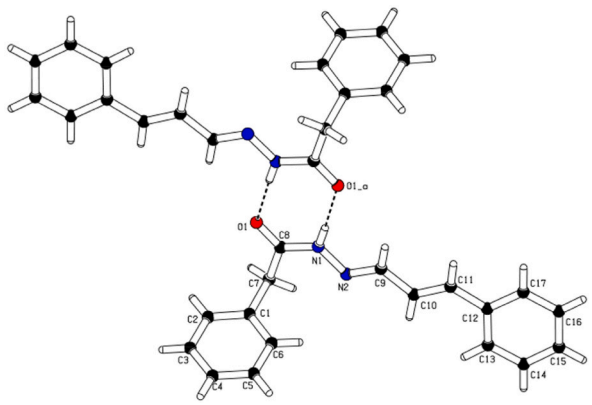

Fig. 9. Dimer formation for the compound PPAH (N1–H1···O1).

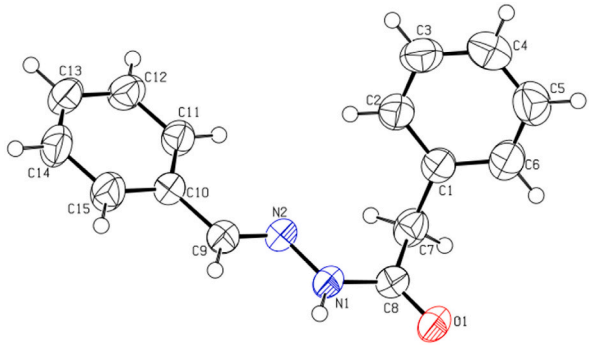

Fig. 10. *ORTEP* diagram of (BPAH), where thermal ellipsoids were drawn at 40% probability level.

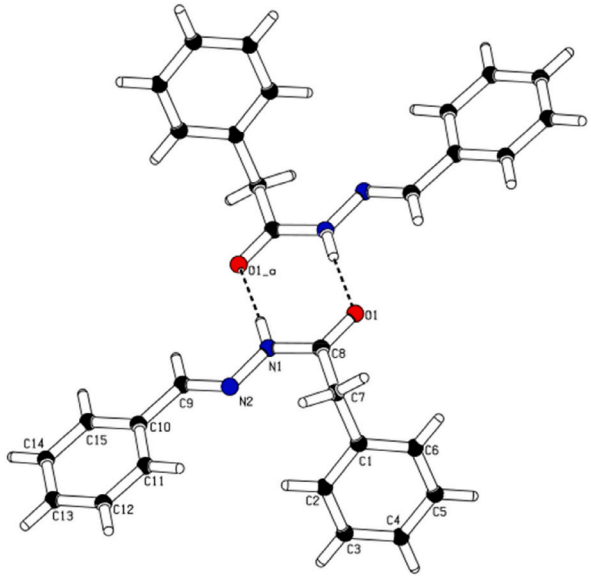

Fig. 11. Dimer formation for the compound BPAH (N1–H1···O1).

Appendix A. Supplementary data

Supplementary data to this article can be found online at https://doi.org/10.1016/j.heliyon.2024.e27303.

References

[1] B.K. Kaymakçioğlu, S. Rollas, Synthesis, characterization and evaluation of antituberculosis activity of some hydrazones, Farmaco 57 (7) (2002) 595–599, https://doi.org/10.1016/S0014-827X(02)01255-7.
[2] J.R. Dimmock, S.C. Vashishtha, J.P. Stables, Anticonvulsant properties of various acetylhydrazones, oxamoylhydrazones and semicarbazones derived from aromatic and unsaturated carbonyl compounds, Eur. J. Med. Chem. 35 (2) (2000) 241–248, https://doi.org/10.1016/S0223-5234(00)00123-9.
[3] A.R. Todeschini, A.L.P. De Miranda, K.C.M. Da Silva, S.C. Parrini, E.J. Barreiro, Synthesis and evaluation of analgesic, antiinflammatory and antiplatelet properties of new 2-pyridylarylhydrazone derivatives, Eur. J. Med. Chem. 33 (3) (1998) 189–199, https://doi.org/10.1016/S0223-5234(98)80008-1.
[4] P.M. Zech Coelho, L. Horacio Pereira, R. Teixeira De Mello, Antischistosomal activity of acridanone-hydrazones in Cebus monkeys experimentally infected with the SJ strain of Schistosoma mansoni, Rev. Soc. Bras. Med. Trop. 28 (3) (1995) 179–183.
[5] M.T. Abdel-Aal, W.A. El-Sayed, E.S.H. El-Ashry, Synthesis and antiviral evaluation of some sugar arylglycinoylhydrazones and their oxadiazoline derivatives, Archiv Der Pharmazie 339 (12) (2006) 656–663, https://doi.org/10.1002/ardp.200600100.
[6] A. Walcourt, M. Loyevsky, D.B. Lovejoy, V.R. Gordeuk, D.R. Richardson, Novel aroylhydrazone and thiosemicarbazone iron chelators with anti-malarial activity against chloroquine-resistant and -sensitive parasites, Int. J. Biochem. Cell Biol. 36 (3) (2004) 401–407, https://doi.org/10.1016/S1357-2725(03)00248-6.
[7] S.G. Küçükgüzel, S. Rollas, H. Erdeniz, M. Kiraz, Synthesis, characterization and antimicrobial evaluation of ethyl 2- arylhydrazono-3-oxobutyrates, Eur. J. Med. Chem. 34 (2) (1999) 153–160, https://doi.org/10.1016/S0223-5234(99)80048-8.
[8] I. Hussain, A. Ali, Exploring the pharmacological activities of hydrazone derivatives : a review Phytochemistry & Biochemistry, Journal of Phytochemistry & Biochemistry 1 (1) (2017) 1–5.

[9] R. Narang, B. Narasimhan, S. Sharma, A review on biological activities and chemical synthesis of hydrazide derivatives, Curr. Med. Chem. 19 (4) (2012) 569–612, https://doi.org/10.2174/092986712798918789.

[10] M. Zhang, Z.R. Shang, X.T. Li, J.N. Zhang, Y. Wang, K. Li, Y.Y. Li, Z.H. Zhang, Simple and efficient approach for synthesis of hydrazones from carbonyl compounds and hydrazides catalyzed by meglumine, Synth. Commun. 47 (2) (2017) 178–187, https://doi.org/10.1080/00397911.2016.1258476.

[11] K.K. Dominik, T.K. Eric, Oximes and hydrazones in bioconjugation: mechanism and catalysis, Chem. Rev. 117 (15) (2017) 10358–10376, https://doi.org/10.1021/acs.chemrev.7b00090.

[12] G. Verma, A. Marella, M. Shaquiquzzaman, M. Akhtar, M.R. Ali, M.M. Alam, A review exploring biological activities of hydrazones, J. Pharm. BioAllied Sci. 6 (2) (2014) 69–80, https://doi.org/10.4103/0975-7406.129170.

[13] O. Pouralimardan, A.C. Chamayou, C. Janiak, H. Hosseini-Monfared, Hydrazone Schiff base-manganese(II) complexes: synthesis, crystal structure and catalytic reactivity, Inorg. Chim. Acta. 360 (5) (2007) 1599–1608, https://doi.org/10.1016/j.ica.2006.08.056.

[14] Y. Lei, T.Z. Li, C. Fu, X.L. Guan, Y. Tan, Synthesis, crystal structures, and antibacterial activity of a series of hydrazone compounds derived from 4-methylbenzohydrazide, J. Chil. Chem. Soc. 60 (2) (2015) 2961–2965, https://doi.org/10.4067/S0717-97072015000200021.

[15] P. Kamur, A. Rai, M. Singh, D. Kumar, A.K. Sahdev, V. Raj, Review on the pharmacological activities of hydrazones derivatives, Ec Pharmaceutical Science 2 (3) (2016) 278–306.

[16] S. Neha, R. Ritu, K. Manju, K. Birendra, A review on biological activities of hydrazone derivatives, Int. J. Pharmaceut. Chem. Res. 8 (3) (2016) 162–166.

[17] D.S.M. Gupta, Synthesis, spectral studies and biological evaluation of hydrazone derivative as antimicrobial and anticancer agents, Int. J. Sci. Res. 7 (10) (2018) 131–137, https://doi.org/10.21275/ART20191633.

[18] J. Wahbeh, S. Milkowski, The use of hydrazones for biomedical applications, SLAS Technology 24 (2) (2019) 161–168, https://doi.org/10.1177/2472630318822713.

[19] P. Krishnamoorthy, P. Sathyadevi, A.H. Cowley, R.R. Butorac, N. Dharmaraj, European Journal of Medicinal Chemistry Evaluation of DNA binding , DNA cleavage , protein binding and in vitro cytotoxic activities of bivalent transition metal hydrazone complexes, Eur. J. Med. Chem. 46 (8) (2011) 3376–3387, https://doi.org/10.1016/j.ejmech.2011.05.001.

[20] J. De Paula, E. Acipreste, H. Maximiler, C. De Paula, R. Soares, A. David, D. Silva, L. Henrique, M. Da, A. Clarissa, Human serum albumin-resveratrol complex formation : effect of the phenolic chemical structure on the kinetic and thermodynamic parameters of the interactions, Food Chem. 307 (September 2019) (2020) 125514, https://doi.org/10.1016/j.foodchem.2019.125514.

[21] S. Mishra, S. Dewangan, S. Giri, S.M. Mobin, Synthesis of Diferrocenyl Hydrazone – Enone Receptor Molecules – Electronic Communication ,Metal Binding , and DFT Study, 2016, pp. 5485–5496, https://doi.org/10.1002/ejic.201601072.

[22] P. Sathyadevi, P. Krishnamoorthy, E. Jayanthi, R.R. Butorac, A.H. Cowley, N. Dharmaraj, Inorganica Chimica Acta Studies on the effect of metal ions of hydrazone complexes on interaction with nucleic acids , bovine serum albumin and antioxidant properties, Inorg. Chim. Acta. 384 (2012) 83–96, https://doi.org/10.1016/j.ica.2011.11.033.

[23] M. Alagesan, N.S.P. Bhuvanesh, N. Dharmaraj, European Journal of Medicinal Chemistry Binuclear copper complexes : synthesis , X-ray structure and interaction study with nucleotide/protein by in vitro biochemical and electrochemical analysis, Eur. J. Med. Chem. 78 (2014) 281–293, https://doi.org/10.1016/j.ejmech.2014.03.043.

[24] R. Sobhy, F. Zhan, E. Mekawi, I. Khalifa, The noncovalent conjugations of bovine serum albumin with three structurally different phytosterols exerted antiglycation effects: a study with AGEs-inhibition, multispectral, and docking investigations, Bioorg. Chem. (2019) 103478, https://doi.org/10.1016/j.bioorg.2019.103478.

[25] J.-H. Shi, et al., Characterization of interactions of simvastatin, pravastatin, fluvastatin, and pitavastatin with bovine serum albumin: multiple Spectroscopic and Molecular Docking, J. Biomol. Struct. Dyn. 35 (7) (2016) 1529–1546.

[26] J.-hua Shi, et al., In vitro study on binding interaction of quinapril with bovine serum albumin (BSA) using multi-spectroscopic and Molecular Docking Methods, J. Biomol. Struct. Dyn. 35 (10) (2016) 2211–2223.

[27] Agilent, CrysAlis PRO, Agilent Technologies, Yarnton, England, 2014.

[28] G.M. Sheldrick, Acta Crystallogr. C C71 (2015) 3–8.

[29] L.J. Farrugia, J. Appl. Crystallogr. 45 (2012) 849–854.

[30] A.L. Spek, Structure validation in chemical crystallography, Acta Crystallogr. D D65 (2009) 148–155.

[31] J.R. Lakowicz, Springer Science & Business Media, 2007.

[32] Q. Wang, et al., Binding interaction of atorvastatin with bovine serum albumin: spectroscopic methods and molecular docking, Spectrochim. Acta Mol. Biomol. Spectrosc. 156 (2016) 155–163.

[33] Sabina Jhaumeer Laulloo, Prakashanand Caumul, Nausheen Joondan, Shobha Jawaheer, Sundev Parboteeah, Sabrina Devi Dyall, Minu Gupta Bhowon, A study of the antibacterial activities and the mode of action of L-methionine and L-cystine based surfactants and their interaction with bovine serum albumin using fluorescence spectroscopy and in silico modelling, Biointerface Research in Applied Chemistry 12 (6) (2022) 7356–7375, https://doi.org/10.33263/BRIAC126.73567375.

[34] S.-B. Kou, et al., Evaluation of the binding behavior of olmutinib (HM61713) with model transport protein: insights from spectroscopic and Molecular Docking Studies, J. Mol. Struct. 1224 (2021) 129024, https://doi.org/10.1016/j.molstruc.2020.129024.

[35] M.N. Arshad, M.M. Rahman, A.M. Asiri, T.R. Sobahi, S.-H. Yu, Development of Hg2+ sensor based on N′-[1-(pyridin-2-yl)ethylidene]benzenesulfono-hydrazide (PEBSH) fabricated silver electrode for environmental remediation, RSC Adv. 5 (2015) 81275—81281.

[36] M.N. Arshad, O. Şahin, M. Zia-ur-Rehman, M. Shafiq, I.U. Khan, A.M. Asiri, S.B. Khan, K.A. Alamry, Crystallographic Studies of Dehydration Phenomenon in Methyl 3-hydroxy-2-methyl-1,1,4-trioxo-1,2,3,4-tetrahydro-1λ 6-benzo[e][1,2]thiazine-3-carboxylate, J. Chem. Crystallogr. 43 (2013) 671–676, https://doi.org/10.1007/s10870-013-0471-5.

[37] M.J. Turner, J.J. Mckinnon, S.K. Wolff, D.J. Grimwood, P.R. Spackman, D. Jayatilaka, M.A. Spackman, Crystal Explorer 17, The University of Western Australia, 2017.